4.2 KrF Laser Driver Options

As described in Section 2.4, the KrF laser was selected as one of the most promising inertial fusion energy (IFE) laser drivers for three principal reasons:

(1) The KrF laser operates at a favorable ultraviolet (UV) wavelength (λ_{KrF} = 248 nm) for inverse Bremsstrahlung coupling to the DT target.
(2) The KrF laser is relatively efficient (ξ = 0.12) for generating UV pulses.
(3) KrF laser amplifiers can be scaled to produce significant UV pulses. (Experimental prototypes have produced as much as 20 kJ.)

There are also some significant drawbacks to the KrF lasers that have been constructed to date. These include:

(1) The KrF laser is a non-storage active medium which, when pumped electrically, means that the duration of the laser pulse is approximately equal to the length of the electrical excitation pulse.
(2) The presently developed type of electrical pulsed power for the KrF is electron-beam excitation which has an optimum pumping pulse duration >600 ns.
(3) E-beam excited excimer lasers have not been demonstrated as being sufficiently reliable to reach the ICF reactor goal of ~10^9 firings between amplifier failures.

Similar comments may be made about the ArF excimer laser (λ = 193 nm) with the additional comments that ArF may be slightly more efficient than KrF owing to a lack of dimer or Kr_2F absorption losses in ArF lasers; but the shorter wavelength coupled with less experimental data on ArF performance in large amplifiers would require additional research to be performed on ArF excimer lasers before recommendations could be made to replace KrF. These two excimer laser media are sufficiently similar that systems originally optimized for KrF may be adapted to use ArF as an alternative gain medium, assuming, of course, that the optical systems were modified to deal with the shorter wavelength (as well as the concomitant hazards of mirror damage, linear absorption, multi-photon absorption, color-center formation, etc.).

It is a given[1] for laser-driven implosion of IFE targets that the laser driver must have a pulse duration, τ_{pulse} ~ 6 ns, an output energy, E_{pulse} 4 to 6 MJ, at a wavelength, λ_{laser} ~ 250 nm, in order to achieve the target irradiation conditions appropriate for efficient implosion of the DT fuel. As is evident from the preceding discussion, the present largest KrF laser prototypes produce pulses of excessive[2] pulse length (~100x) and inadequate[3,4,5] energy (~10%) for a 25-beam (200 kJ/beam) ICF laser driver.[6,7,8] Thus, a future KrF laser driver[9,10] suitable for IFE reactor operation will need to produce efficient shorter UV laser pulses at higher energies.

Another problem common to all large aperture, high energy lasers is the large aperture optics problem. Optical elements (particularly UV optical elements) become very expensive for elements larger than ~50 cm. On the basis of the volumetric cost of the optics alone, scaled optics of aperture, d, have costs proportional to d^3. Typically, the manufacture of larger optics exhibit a lower yield than smaller optics so that, in fact, the costs for large optics scale, with exponents ranging from 3.5 to 7 depending upon yield, grinding and polishing hazards, coating problems, etc. If a large optic of aperture D is synthesized by n^2 subapertures of diameter d (where n = D/d), then the costs of the synthesized optic would be proportional to D^2. Since UV optical damage thresholds tend to limit the maximum laser fluence, Φ_{laser}, tolerable to values ~5 J/cm^2, in order to generate laser pulses of 5 MJ, effective apertures having collective areas of ~10^6 cm^2 for the laser will be required. The costs associated with procuring this large optical surface area can be minimized if the required apertures (and corresponding optical component areas) are synthesized from smaller, cost and performance-optimized optical elements.

After reviewing the KrF laser amplifier literature2-10 and performing our own optimization analyses, we have found that potentially more reliable and efficient excimer laser amplifiers having apertures of ~30x30 cm may be feasible9,10. Accordingly, the fundament of our IFE design for the KrF laser driver is that the most efficient, reliable, cost-effective excimer laser amplifier produces a laser beam of reduced energy (E_{laser} ~ 4 kJ) using an electric discharge excimer laser (EDEL) excitation scheme9,10 which, even with an optimized electrical excitation pulse shape, has a duration too long (EDEL ~ 250 ns) to be useful as a laser driver in IFE target implosions. As a consequence, in order to exploit the high efficiency and cost effectiveness of optimized EDEL amplifiers,9,10 it was necessary to develop: (1) a laser beam combination system to synthesize higher energy laser beams than can be achieved efficiently in a single laser amplifier, and (2) a pulse compression system to shorten the optimum EDEL pulse to the required duration.

There are two general types of optical beam combinations and pulse compressions which have been studied[10-13] during the past decade: linear (use of linear optics, such as lenses and mirrors, to effect parallel beam combination; use of a mirror-based geometry referred to as "angular multiplexing" for temporal pulse compression) and non-linear (Raman beam combination, non-linear optical pulse compression) laser beam configurations.

Linear laser beam manipulation techniques[7,8,9] utilize, by definition, linear optical elements (such as lenses, mirrors, beam-splitters, etc.) to accomplish the objectives of beam combination and pulse compression using long pulse excimer laser light as input. Although typically large numbers of optics and generous amounts of real estate are required, this approach may have advantages since it is fundamentally simple and the spectral bandwidths of potentially wide-bandwidth excimer laser beams are

generally unaffected by linear beam manipulation processes. A major disadvantage of linear beam manipulation techniques is that their optical complexities are approximately proportional to the number of beams to be accumulated or the pulse compression factor.

Non-linear laser beam manipulation[10-18] employs advances in innovative non-linear optical (NLO) processes to accomplish the objectives of beam combination and pulse compression using stimulated quantum mechanics techniques. These NLO processes promise to achieve not only the general objectives of laser beam combination and pulse compression with much simpler optical configurations, but also to smooth excimer laser spatial intensity distributions and improve the accumulated laser beam quality. Given the significant advances demonstrated in the laboratory during the last decade, all of these advantages may be achieved while reducing both cost and risk. Lastly, NLO processes are able to accommodate significant changes in the number of laser beams to be accumulated, or in the pulse compression factor, without substantial changes in configuration or design. Both linear and NLO laser beam manipulation techniques will be described in additional detail in the discussions below.

4.2.1 Linear Optical Manipulation Techniques - In order to allow the KrF laser amplifiers to meet the fundamental fusion target irradiation requirements, two major goals must be achieved: (1) beam combination, and (2) pulse compression. Beam combination is necessary in order to permit the addition of a large number of optimized laser beams to achieve the required laser energy per beam line. This permits the optimization of the output energies of individual excimer laser modules (discussed below in Section 4.2.2) while meeting the requirements for achieving a specific laser energy delivered per individual laser beamline. Thus, for example, if the Prometheus design would require a 6 MJ laser driver delivering the 6 MJ of energy in 60 beam lines, each laser beam line requires laser pulses of approximately 81 kJ each. If, however, the optimization of the excimer laser amplifiers produces a design which is capable of producing only 5kJ/amplifier, then it will be necessary to combine at least 20 such excimer laser beams in order to reach the required energy level of 81 kJ for each beamline.

In an analogous manner, pulse compression can be achieved using linear optics by synthesizing a long pulse of duration, $N\tau$, from a series of N shorter pulses, each of duration τ, and propagating at unique angles, θ_k, to the system axis.[2-8]. In this connection, linear pulse compression techniques (i. e., angular multiplexing) are increasingly difficult to utilize as N increases. Thus, since the optimum pumping pulse duration of the EDEL[9,10] is approximately half that of the EBEL,[2] the angular multiplexing system for the EDEL would have less than half the number of beam lines as the corresponding system for the EBEL. Each of these linear beam combination techniques is briefly described below.

Use of linear optical elements, including lenses, mirrors, beamsplitters, optical delay lines, and adaptive optics, permit the spatial and temporal manipulation of high power laser beams. By linear optical elements, it is understood that these optical elements function substantially in the same manner for laser beams of low intensity as well as laser beams at high intensity.

4.2.1.1 Linear Beam Combination - Linear beam combination is a process which involves directing the output beams of individual laser amplifiers using appropriate mirrors and beamsplitters to accomplish the following objectives:

(1) Accumulate the requisite energy in a series of nxn parallel-propagating beams which, when summed, form an array whose beam diameter is sufficiently large to avoid optical damage to the mirrors and windows in the optical train.

(2) Be timed such that the net path delays among all of the beamlets are significantly less than 1 ns. (This techique may involve phase-matching the individual beamlines using linear adaptive optics techniques.)

(3) Be directed within an alignment angle of the order of the diffraction-limited divergence of the array elements themselves.

The advantage of this type of linear beam combination is that it does not adversely affect the spectral bandwidth of the excimer laser light. The major disadvantage is that the optical system suitable for combining the laser beams tends to be relatively large and unwieldy; difficulties also arise with regard to beam fill factors and near field (Fresnel) diffraction effects from the "egg-crate" multiple mirror mounts unless image relaying is employed.

4.2.1.2 Angular Multiplexing - Linear pulse compression has some of the same characteristics as linear beam accumulation, except that each beamline is injected through the laser amplifiers at a different angle of incidence. This leads to a significantly more complicated optical design, as discussed below.

Previous IFE KrF driver designs[3-8] have featured an optical technique known as angular multiplexing to accomplish the important task of reducing the optimum pulse length for excimer laser amplifiers, $\tau_{excimer}$ ~ 250 ns, by approximately a factor of 45 to meet the target illumination requirement of τ_{pulse} ~ 6 ns. Although this technique is attractive for relatively small compression ratios (<20), complexities arise when compression ratios of >40 are needed. As discussed in Section 6.5.1.2, optimized electric discharge excimer laser (EDEL) amplifiers[9,10] produce pulse durations of ~250 ns, whereas optimized e-beam excited excimer laser (EBEL) amplifiers[2] generate pulses of ~600 ns. In the latter case, angular multiplexing would need to generate a pulse compression ratio of ~100 in order to meet the requisite compressed

pulse duration. A schematic of the angular multiplexing pulse compression concept is shown in Figure 4.2.1-1.

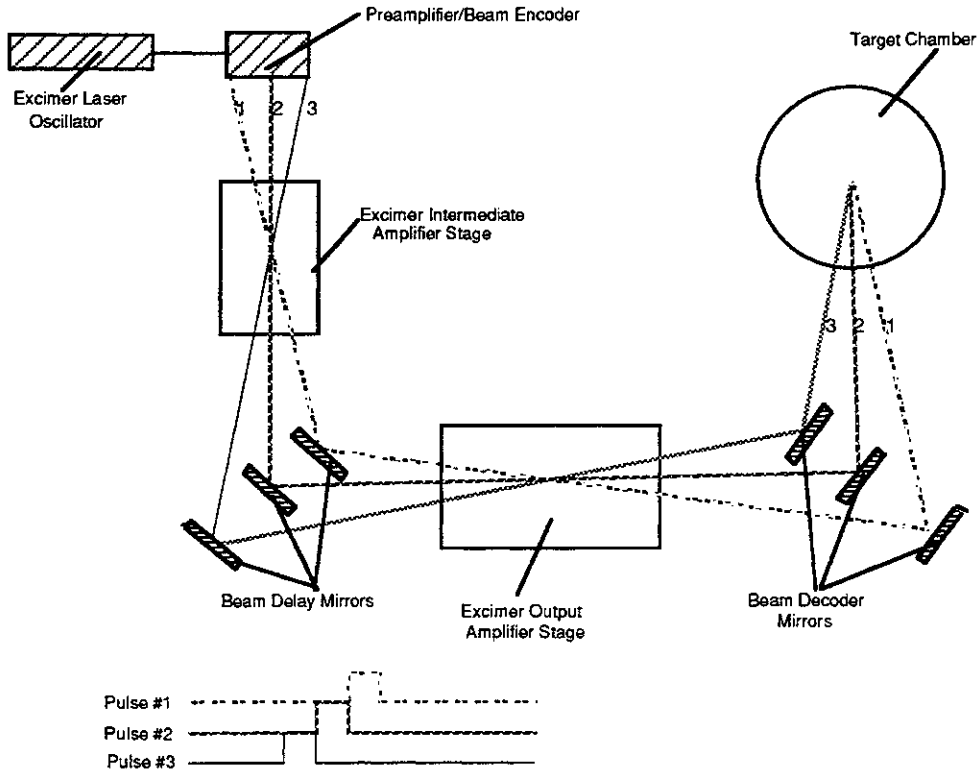

Figure 4.2.1-1 Angular Multiplexing is Accomplished by Synthesizing a Long Laser Pulse from a Series of Suitably Delayed Shorter Laser Pulses Each Propagating at a Specific Angle With Respect to the Optical Axis of the System

Figure 4.2.1-1 illustrates the angular multiplexing concept when a pulse compression of three is desired. As previously discussed, the number of angular-encoded sub-beams required in an angular multiplexer is equal to the pulse compression ratio. Thus, when a pulse compression factor of 100 is required, 100 separate, angular-encoded beam lines (each propagating at a unique angle relative to the system axis) are needed for the angular multiplexing system. Even with careful design, angular multiplexing for large compression factors may result in an unwieldy optical configuration; for small interbeam angles, cross-talk problems between adjacent channels can occur; and unextracted excimer laser volumes can result since beam vignetting occurs. This design does, however, permit broad-bandwidth excimer laser pulses to be compressed while retaining the large bandwidths, a property useful for minimizing adjacent beam interference effects on the target and reducing stimulated scattering processes in plasma atmospheres ablated from targets.

4.2.2 Non-Linear Optical Beam Manipulation Processes - Both of our Prometheus studies and numerous publications[10-17] have shown that two different types of non-linear optical (NLO) systems can be used to accomplish the tasks of

beam combination and pulse compression with both relatively high efficiency (>50%) and flexiblity. Whereas for the linear beam manipulation techniques, there is a proportional penalty for the degree to which (i. e., n beams) beam accumulation is necessary or the fractional pulse compression ratio (i. e., 1/n), for the NLO approaches, it is generally an easier task to accommodate increases (or decreases) in the number of beams to be accumulated or pulse-compressed. Thus if n beams are to be accumulated, the linear optical approach requires n parallel optical systems; whereas the NLO accumulator simply combines n excimer pump beams into a single output beam. Similarly, if the desired pulse compression ratio is n, then the angular multiplexing pulse compressor requires n separate beam lines, each at a separate angle, whereas the NLO compressor performs the pulse compression in a single beam line folded back upon itself.

Each of these systems is briefly described below.

4.2.2.1 NLO Laser Beam Combination - This section will summarize the Prometheus architecture of the non-linear optical beam combination system based on forward rotational Raman scattering.[10,15] As previously discussed, beam combination gives the laser designer the important option to optimize the performance of the excimer laser amplifiers independently of the overall IFE reactor system requirements to deliver a specific amount of laser energy in each beamline to the target. Thus, were it not for the concept of coherent beam combination, it would be necessary to deliver some 81 kJ in each beamline to the target. For coherent beam combination, this might mean, for example, that the 81 kJ of energy would have to be delivered from a single excimer laser amplifier; a feat which has not yet been demonstrated.[5,9] Moreover, the single point failure of any one of these 60 large excimer laser amplifiers would cause the misfiring of the fusion target on that (and presumably successive) shots, thereby forcing the shutdown of the IFE reactor.

During the study, the design architecture for the Raman accumulator system has evolved from earlier considerations of extremely large e-beam pumped excimer lasers (producing 50 to 100 kJ each) to the present conservative (~4 kJ) pump excimer laser amplifier–forward rotational Raman accumulator system. These Raman accumulators work well with either the 600 ns pulse durations of the EBELs or the ~ 250 ns pumping pulse durations of the EDELs. The fundamental purpose of the forward rotational Raman accumulator is coherent beam combination in which a number (e. g., 4x4 = 16) of excimer laser beams of modest energy (~6 kJ) and aperture (~30 cm) are combined into a high energy beam (~81 kJ) and relatively large aperture (~120 cm). In order to achieve a high quantum efficiency, ξ, it is convenient to select specific rotational Raman transitions in hydrogen (or deuterium). The Raman convertor quantum efficiency, ξ, is defined by the expression:

$$\xi = \frac{h\nu_{laser} - \Delta E_{rot}}{h\nu_{laser}} \qquad (4.2.2\text{-}1)$$

where h is Planck's constant, ν_{laser} is the frequency of the excimer laser, and ΔE_{rot} is the energy of the rotational Raman phonon. In order to achieve the highest Raman gain, the polarization state of both the excimer pump beam and the Stokes seed beam must be circular and of opposite helicities. As an example, for two such rotational transitions in room temperature hydrogen, values of $\Delta E \sim 587\ cm^{-1}$ (for S[1]–S[3]) and $354\ cm^{-1}$ (for S[0]–S[2]) have been measured. The relationship of the Stokes seed wavelength, λ_S, to the laser wavelength, λ_{laser}, is given by the simple expression:

$$\lambda_S = \frac{\lambda_{laser}}{\xi} \qquad (4.2.2\text{-}2)$$

where ξ is defined in Eq. 4.2.2-1. Since for $\lambda_{laser} \sim 248$ nm there is only a very slight wavelength difference between λ_{laser} and λ_S, it is difficult to separate the pump and Stokes seed beams spectrally. However, by injecting the Stokes seed beam at an angle θ to the excimer pump beam(s), it is possible to inject the Stokes seed beam efficiently into the Raman accumulator cell. Moreover, intensity averaging occurs under these circumstances, which can lead to an improvement[10,14,15] in Stokes beam quality compared to that of the excimer laser pump. An example of how this beam combination task might be accomplished is shown in Figure 4.2.2-1.

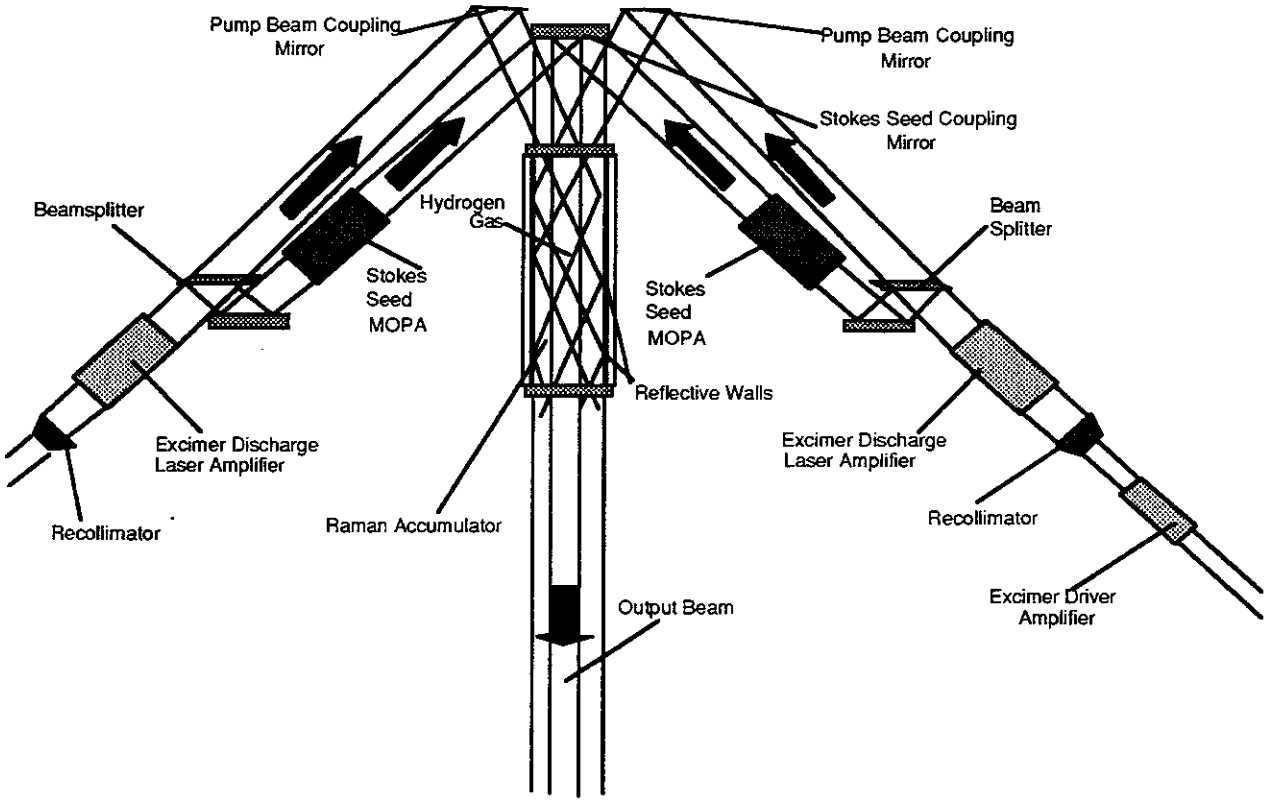

Figure 4.2.2-1 The Forward Rotational Raman Accumulator Permits 16 Separate KrF Laser Beamlets to be Combined in a Single Coherent Beam

The crossed Raman (or CRAM) configuration illustrated schematically in Figure 4.2.2-1 provides an example of a Raman seed beam derived from the original excimer pump, thereby guaranteeing that the highest Raman gain will be achieved. To achieve high gain with the bandwidth of the excimer pump greater than the Raman linewidth, this configuration requires that the optical path length of the seed generator be matched to the main excimer pump path length.[14] In this case, the optical gain, G_R, of the Raman amplifier is given by the expression:

$$G_R = \exp\left[g_R(\rho,\theta)\, I_{laser} L_{interaction}\right] \qquad (4.2.2\text{-}3)$$

where $g_R(\rho,\theta)$ is the rotational Raman gain coefficient (dependent upon the gas density, ρ, and the angle between the pump and Stokes beams, θ). An important parameter in stimulated Raman scattering is the bandwidth, $\Delta\nu_R$, of the Raman transition. An expression[15] for the Raman bandwidth, $\Delta\nu_R$, is:

$$\Delta\nu_R = \frac{K_1 \left|K_p - K_s\right|^2}{\rho} + K_2\rho \qquad (4.2.2\text{-}4)$$

where K_1 and K_2 are two constants which depend upon the Raman medium, ρ is the medium density in amagat, K_p is the pump wave vector, and K_s is the Stokes wave vector. In turn, the rotational Raman gain coefficient, g_R, is dependent[10,15] upon Raman bandwidth, $\Delta\nu_R$, the gas density, ρ, and the angle, θ, according to the expression:

$$g_R = \frac{2\lambda_s^2 \Delta N}{h\upsilon_p \pi \Delta\nu_r(\theta,\rho)} \frac{d\sigma}{d\Omega} \qquad (4.2.2\text{-}5)$$

where λ_s is the Stokes wavelength, ΔN is the density of scatterers, $h\nu_p$ is the quantum pump energy, $\Delta\nu_r(\theta,\rho)$ is the Raman linewidth, and $d\sigma/d\Omega$ is the differential cross-section for rotational Raman scattering. A plot of the dependence of g_R on ρ and θ is illustrated in Figure 4.2.2-2 for $\lambda_{laser} \sim 248$ nm, $\theta = 0°$, 5°, and 10°.

As indicated in Figure 4.2.2-2, for $\theta \sim 10°$, a significant reduction in $g_R(\theta)$ is observed for densities of $H_2 < 1.5$ amagat. As a consequence, we have considered using angles smaller than $\theta = 10°$ (i. e., $\theta = 5°$) if gas pressures above 1 atm are to be avoided. High H_2 pressures lead to the requirement for thick Raman cell windows and produce higher relative optical gains for competing vibrational Raman transitions (for $\rho > 2$ amagat).

As an illustration of the effect the Raman gain coefficient has on the predicted conversion efficiency of the accumulator, plots of the conversion efficiency vs. Raman cell length for the S(1) rotational hydrogen Raman with $\lambda_{laser} = 248$ nm, $E_{laser} = 4$ kJ, $D_{beam} = 30$ cm, $\tau_{pulse} = 600$ ns, ρ ranging from 1.0 to 2.0 amagat, and θ ranging from 5 to 10° are illustrated in Figure 4.2.2-3.

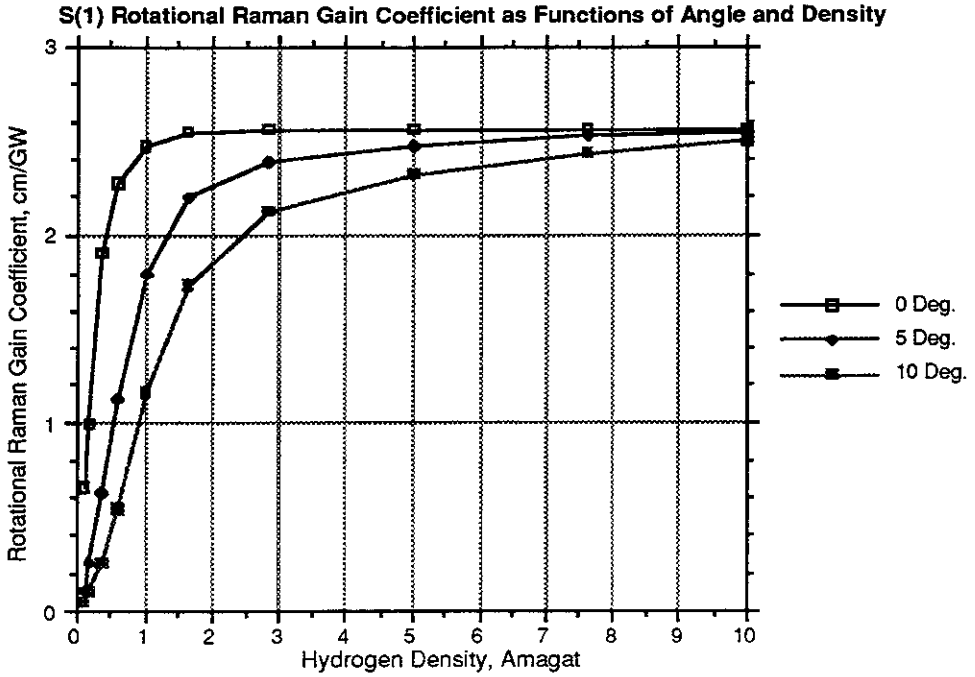

Figure 4.2.2-2 S(1) Rotational Raman Gain Coefficient as a Function of ρ for Different Values of CRAM Angle, θ

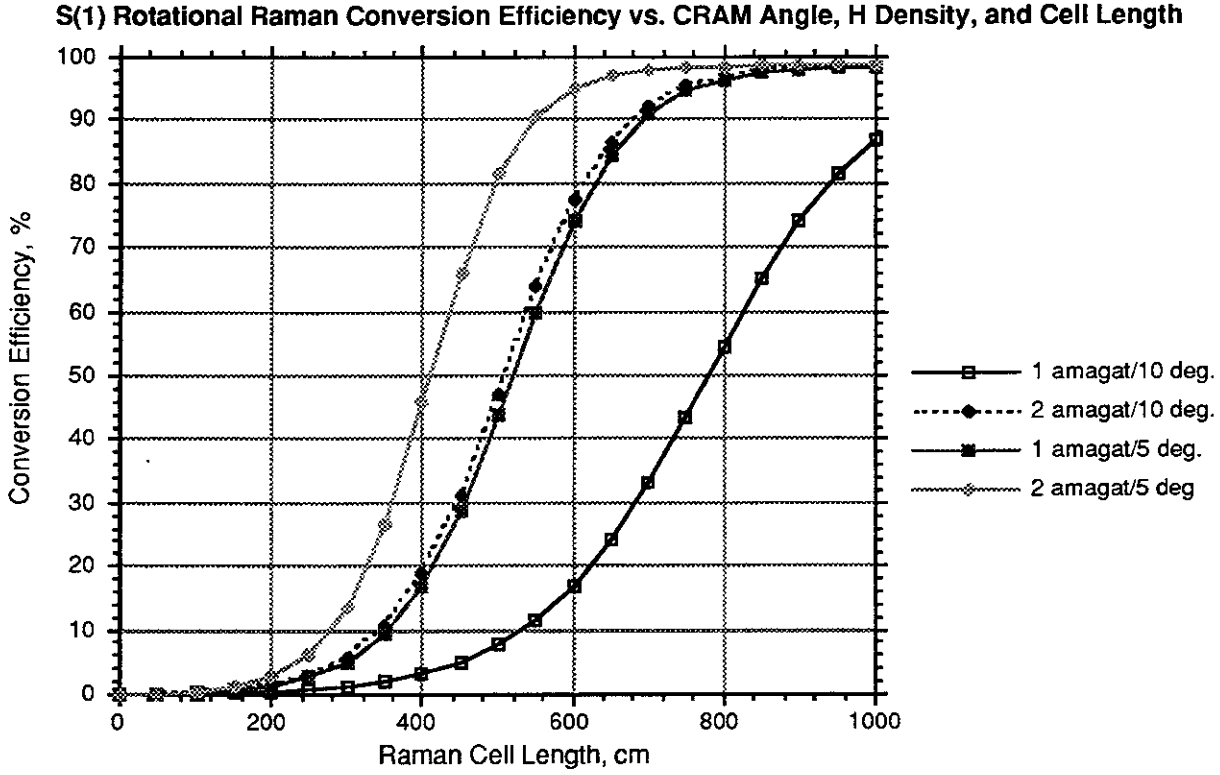

Figure 4.2.2-3. Accumulator Conversion Efficiencies as a Function of Cell Length with ΔE = 4 kJ, D_{amp} = 30 cm, τ_{pulse} = 600 ns, and λ_{laser} = 248 nm

As indicated, for $\theta = 10°$ and $\rho = 1$ amagat, 90% conversion is not achieved for $L < 1000$ cm, whereas for $\theta = 5°$ and $\rho = 2$ amagat, 90% is achieved at $L = 530$ cm. The axial ($\theta = 0$) small signal Raman gain given by Eq. 4.2.2-5 ranges from 10 nepers for $L = 500$ cm (acceptable) to 20 nepers for $L = 1000$ cm (marginal). It would be preferable if high conversion efficiencies ($\xi_R > 90\%$) can be achieved for interaction lengths, $L < 6$ m. In the present case, the fluence on the cell windows is only 4.4 J/cm^2. Higher fluences (either smaller beam diameters or higher energies) would permit efficient beam conversion in shorter distances. If higher energies can be achieved in the electric discharge excimer lasers (i. e., $\Delta E = 4.8$ kJ), then efficient conversion in the Raman accumulator cells can be achieved in a shorter distance. These results are shown in Figure 4.2.2-4.

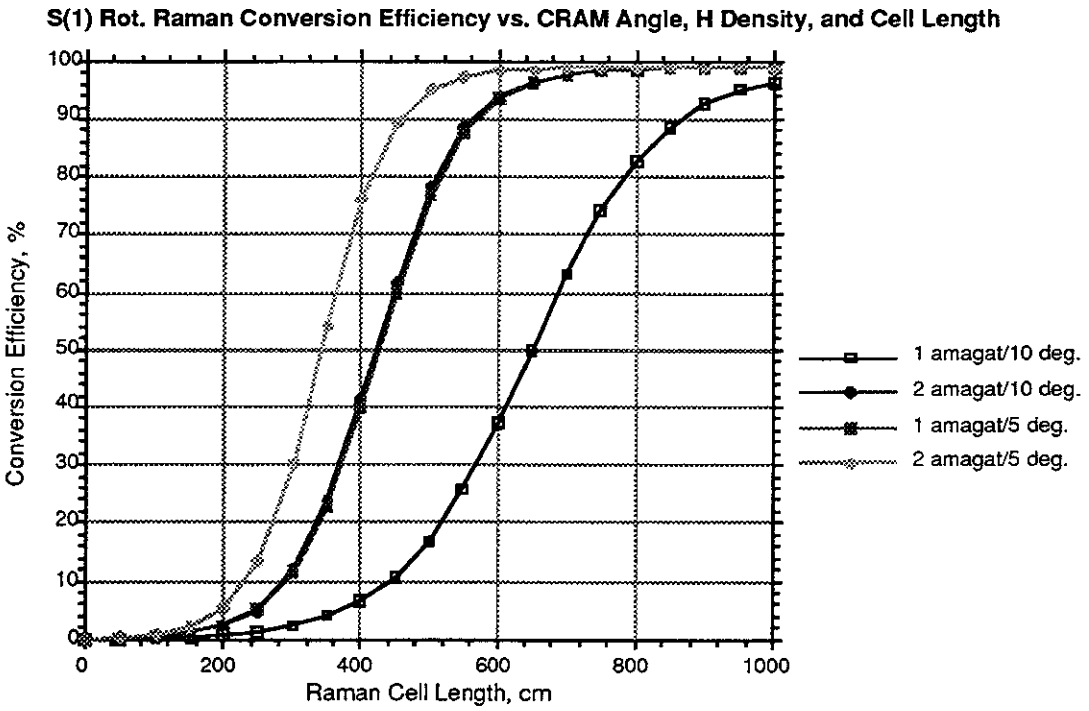

Figure 4.2.2-4 The Accumulator Conversion Efficiency Depend on the Raman Cell Length with $\Delta E = 4.8$ kJ, $D_{amp} = 30$ cm, $\tau_{pulse} = 600$ ns, and $\lambda_{laser} = 248$ nm

In this case, with a modest increase to a flux loading of 5.3 J/cm^2, a reduction in Raman cell length could be achieved. This increase in fluence could be achieved either by increasing the excimer output energy, ΔE, from 4 to 4.8 kJ, or by decreasing the amplifier aperture slightly, from 30 cm to 27.5 cm. As indicated, for $\theta = 10°$ and $\rho = 1$ amagat, 90% conversion is attained only for $L = 860$ cm, whereas for $\theta = 5°$ and $\rho = 2$ amagat, 90% is achieved at $L = 440$ cm. The axial Raman gain ($\theta = 0$) in this case for $L = 500$ would be approximately 12 nepers. These considerations apply primarily to Raman conversion of a single e-beam excimer laser (EBEL) amplifier, since EBEL laser amplifier pulse lengths are relatively long (~600ns). For electric-discharge excimer laser (EDEL) amplifiers, a shorter (~250 ns) pulse duration appears to be more optimum. These shorter duration, proportionally higher output power

pulses produce higher Raman gains. Shown in Figure 4.2.2-5 are Raman accumulator cell (RAC) conversion efficiency curves for 4x4x6 kJ EDEL pump amplifiers (~81 kJ) delivered to the RAC in a pulse duration of 250 ns. This represents the Prometheus-L laser driver design point.

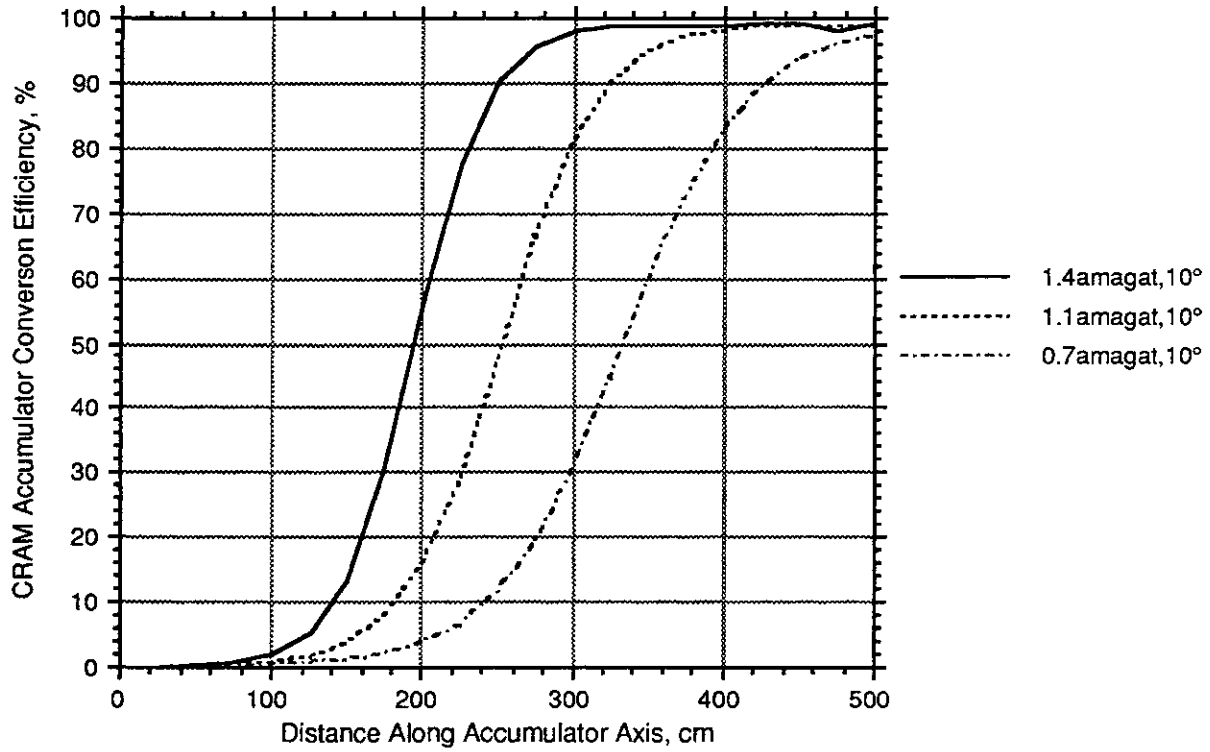

Figure 4.2.2-5. With an Input of 81 kJ in a 250 ns Pulse for λ = 248 nm in Deuterium at Sensitivities of 0.7, 1.1, and 1.4 amagat with the CRAM Angle = 10°, the Conversion Efficiency Depends Upon the RAC Length.

It is important not to exceed Raman conversion efficiencies greater than ~90% since the danger arises that some conversion to higher order Stokes lines could occur. Under controlled conditions (i.e., deliberately injecting a second Stokes seed), this could permit an increase in the effective bandwidth of the RAC laser beam since it would contain two discrete wavelengths (corresponding to the first and second Stokes order in D_2). The separation of wavelengths would depend upon whether the Raman lines selected were rotational or vibrational. If, for example, the S(2)–S(0) rotational transition in hydrogen were optimized ($\Delta E \sim 354\ cm^{-1}$), then the wavelengths of the first and second Stokes would be 250.2 and 252.4 nm (separated by 2.2 nm), assuming that the 248 nm KrF laser were used as a pump. If the S(3)–S(1) rotational transition in hydrogen were optimized ($\Delta E \sim 587\ cm^{-1}$), then the first and second Stokes would lie at 251.6 and 255.2 nm (separated by 3.6 nm). These Raman lines would represent 0.87 and 1.45% bandwidths, respectively.

In addition to the simulations of RAC performance for KrF laser pumps, a number of Raman conversion calculations were carried out assuming that ArF (λ = 193 nm) were the pump wavelength. It should be noted that, if further excimer laser research revealed that ArF were a superior excimer gain medium to KrF but that problems associated with two-photon absorption and/or color center formation in transmissive optics made operation at λ_{laser} = 193 nm unattractive, using the Q(1) vibrational transition in H_2 (corresponding to a phonon energy of 4155.2 cm^{-1}) or the Q(2) vibrational transition in D_2 (for an energy shift of 2987.2 cm^{-1}) would permit the Stokes output wavelength from the accumulators to be either λ_{Stokes} = 210 nm (for H_2) or λ_{Stokes} = 205 nm (for D_2); these longer wavelengths may prove to be an acceptable compromise between 248 and 193 nm.

4.2.2.2 Backward Raman Pulse Compression - As discussed above, as a consequence of the complexity of angular multiplexing as applied to the present problem, other pulse compression techniques were examined. Two different methods which use non-linear optical techniques were considered:

(1) Backward stimulated Raman scattering (SRS) pulse compression.[11,12]
(2) Backward stimulated Brillouin scattering (SBS) pulse compression.[10,15,17]

These non-linear pulse compressors both utilize stimulated scattering processes which are capable of using the long pulse excimer laser pump beams for efficient conversion to higher radiance Stokes beams with differing wavelengths, directionality, phase aberrations, and temporal durations. Because these non-linear optical techniques are enormously flexible, such a dual-architecture system permits a wide variety of pulse shapes, wavelengths, etc., to be achieved without requiring any significant changes in the overall system configurations.

A schematic of a backward Raman pulse compressor[11,12] is illustrated in Figure 4.2.2-6.

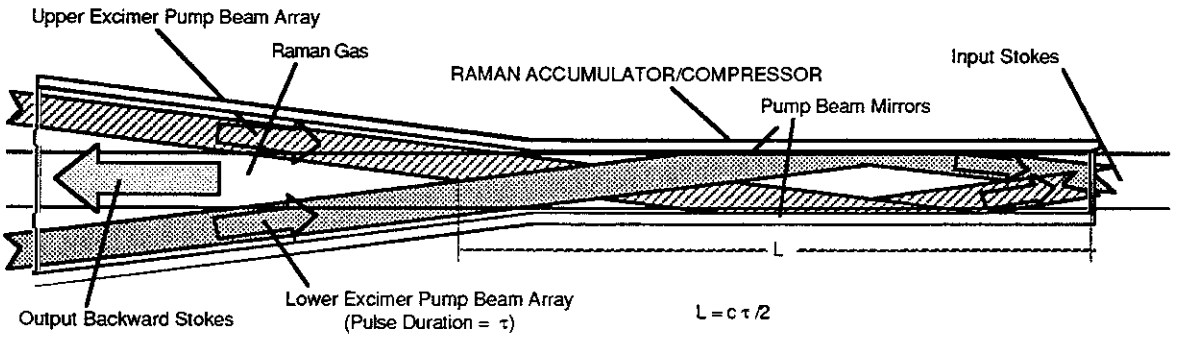

Figure 4.2.2-6 The Backward Raman Pulse Compressor Overlaps the Long Excimer Laser Pulse with a Shorter, Backward-Propagating Stokes Seed to Achieve Pulse Compression.

As indicated in Figure 4.2.2-6, a Raman cell having a length, $L_R = c\tau_{laser}/2$, has a Stokes seed of wavelength, λ_S (defined in Eq. 4.2.2-2). Although such a device can accomplish both the functions of beam accumulation and pulse compression, experiments and analyses have shown that backward Raman pulse compression typically can achieve efficient operation only for pulse compression factors of 5 or less.[11,12] Thus, in order to achieve an overall pulse compression of 100, it would be necessary to have three successive backward Raman pulse compressors. Hitherto, this has been an unattractive solution because of the reduced overall conversion efficiency.

4.2.2.3 SBS Pulse Compression - A third pulse compression technique utilizing stimulated Brillouin scattering (SBS) has been considered for performing the function of laser pulse compression. The SBS process[10,16,17] exhibits optical gain in a functional form similar to that given for SRS Eq. 4.2.2-3 as shown in Eq. 4.2.2-6:

$$G_{SBS}(\rho, \Delta\nu, t) = \exp\left(g_{sbs}[\rho, \Delta\nu]\, I_{laser}(\Delta\nu, t)\, L_{cell}\right) \qquad (4.2.2\text{-}6)$$

where the SBS gain coefficient, $g_{SBS}(\rho,\Delta\nu_{pump})$, is primarily a function of the gas density and the bandwidth of the pump laser, $\Delta\nu_{pump}$. The physics of SBS differs from that of SRS in that the scattering of incident excimer laser photons from sound waves in the SBS medium occurs, as compared with the scattering of light from molecular energy states, as the basis of the SRS process. The difference in frequency between the excimer laser, ν_{laser}, and the Stokes seed, ν_{SBS}, is simply the Doppler shift, $\Delta\nu_D$, suffered by the pump photons when scattered from the moving density waves in the Brillouin gain medium. Thus, $\Delta\nu_D = 2\nu_{laser}v/c$ where v is the sound speed in the SBS medium and c is the speed of light. As a result, the quantum efficiency for the SBS process defined in Eq. 4.2.2-6 can be very high, $\xi \sim 100\%$.

The Brillouin gain coefficient, g_B, is defined by the relation:[16]

$$g_b = \frac{k_s^2 \gamma_e^2}{nc\nu_s \rho \Gamma_B} \qquad (4.2.2\text{-}7)$$

where k_s is the wave vector of the Stokes beam, γ_e is the electrostrictive coefficient (of the SF_6 SBS gain medium), n is the refractive index, c is the speed of light, v_s is the speed of sound in the gas, ρ is the density, and Γ_B is the spontaneous Brillouin linewidth.

Building upon the work of Mak,[17] et al. in the Soviet Union, we have analyzed the case in which the leading edge of the long, 600 ns excimer laser pulse is electronically chirped in frequency by an amount equal to the SBS seed frequency, $\Delta\nu_{SBS}$, and then ramped in modulation depth to encourage the generation of pulses >1 ns duration. We then have a very flexible method of generating a variety of output compressed

pulse shapes in a single non-linear, self-seeding, pulse compressor. A schematic of the SBS pulse compression concept is shown in Figure 4.2.2-7.

It is assumed that the SBS pulse compressor has, as an input beam, a long pulse (τ_{pulse} ~ 600 ns) output beam from a Raman accumulator. This long pulse beam is shown as the first waveform in Figure 4.2.2-7. The first step in the SBS pulse compression process[17] is to "chirp" the first few nanoseconds of the leading edge of the long, τ_{laser} ~ 600 ns laser pulse originating in the Raman accumulators (described above). In Step II, this long laser pulse with the "chirped leading edge" is then directed into a gas-filled SBS cell of approximate length $L = c\tau_{laser}/2$ equipped with a 100% reflecting mirror at the far end of the cell. The purpose of this mirror is to reflect the short duration, "chirped" SBS "seed" beam back down the cell where the high, stimulated Brillouin gain can effect an efficient conversion of long pulse energy into a short pulse Stokes beam. Thus, upon reaching the 100% mirror and being retroreflected, the chirped leading edge of the excimer pulse serves as the SBS Stokes "seed" beam to extract the majority of the power in the original long pulse excimer beam in a time, $\tau_{pulse} << \tau_{laser}$. Since the characteristics of this "chirped" SBS seed are electronically determined, this method permits a wide variety of pulses to be generated. An operational diagram of how such pulse compressors could be configured is shown in Figure 4.2.2-8.

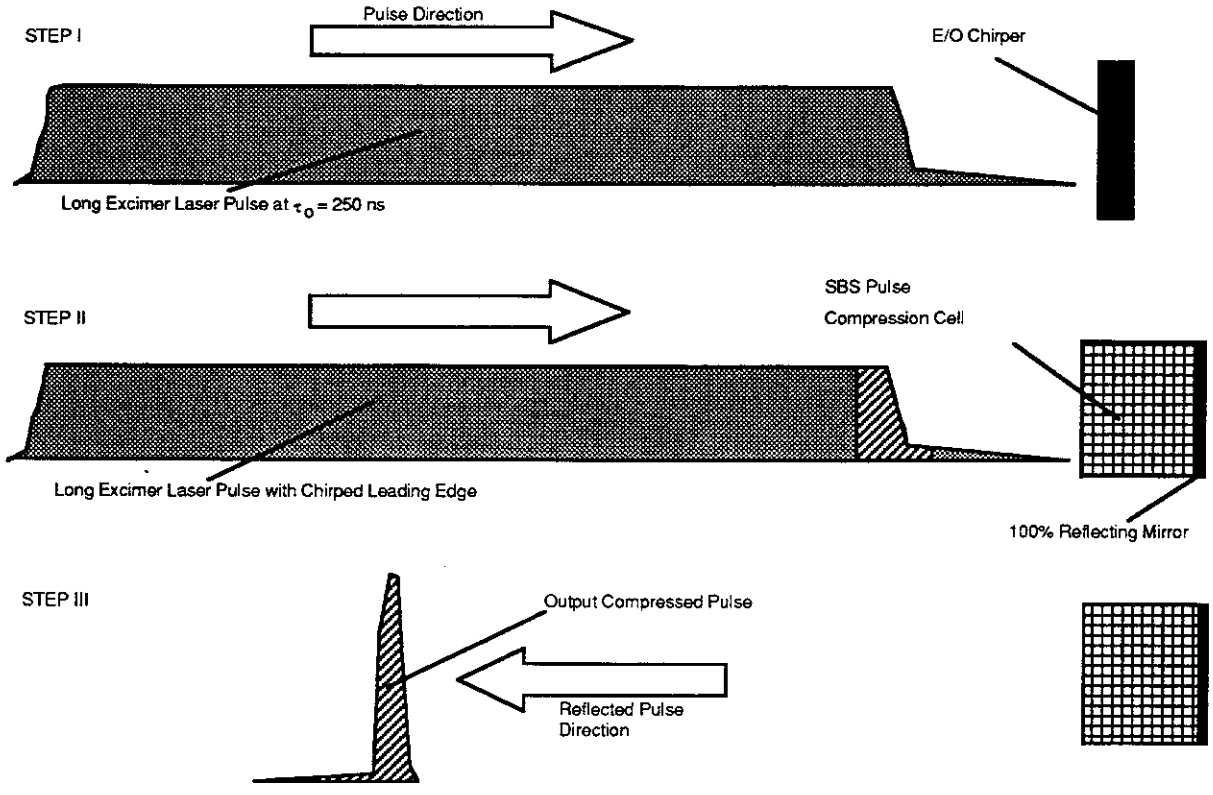

Figure 4.2.2-7 The Three Steps Associated with Pulse Compression in the SBS Pulse Compressor.

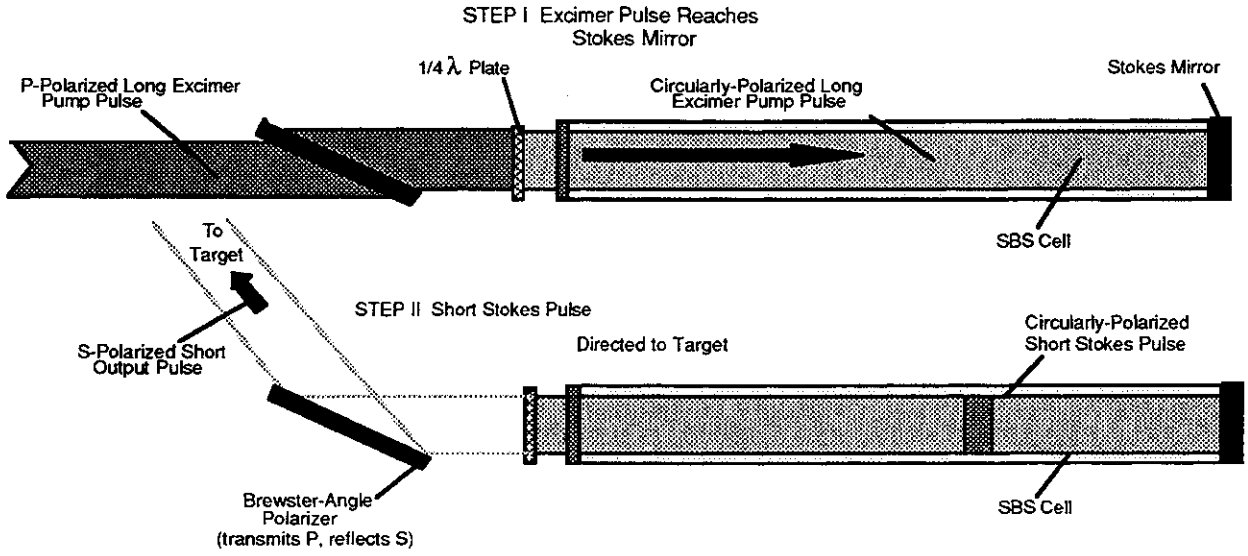

Figure 4.2.2-8 Use of SBS Pulse Compressor Cell Coupled With Polarized Input and Output Laser Beams Facilitates Integration into Reactor

As indicated in Figure 4.2.2-8, the use of linearly-polarized light, together with a large aperture, dielectric-polarizer, and a quarter-wave plate, permits the long pulse input and short pulse output beams to be readily separated with high efficiency. It is not convenient to separate the compressed pulse from the input long pulse spectrally because the SBS frequency shift is nearly negligible in comparison with the laser frequency. Similarly, it is generally not convenient to have a significant angle, θ, between the temporally long incident pump pulse and the short Stokes compressed pulse because poor spatial overlap would then occur with a concomitant reduction in conversion efficiency. A schematic of the placement of the SBS pulse compressor relative to the Raman accumulators is illustrated in the diagram shown in Figure 4.2.2-9.

One of the useful properties of these non-linear devices (i. e., the Raman accumulators and the SBS pulse compressors) is that essentially none of the excimer laser light is lost in the devices. Any laser light that is not converted can be collected and put to additonal uses, recirculated, etc. In this case (shown in Figure 4.2.2-9), any long pulse excimer laser power not converted in the Raman accumulator cells would be available for generating complex pulse shapes for target illumination.

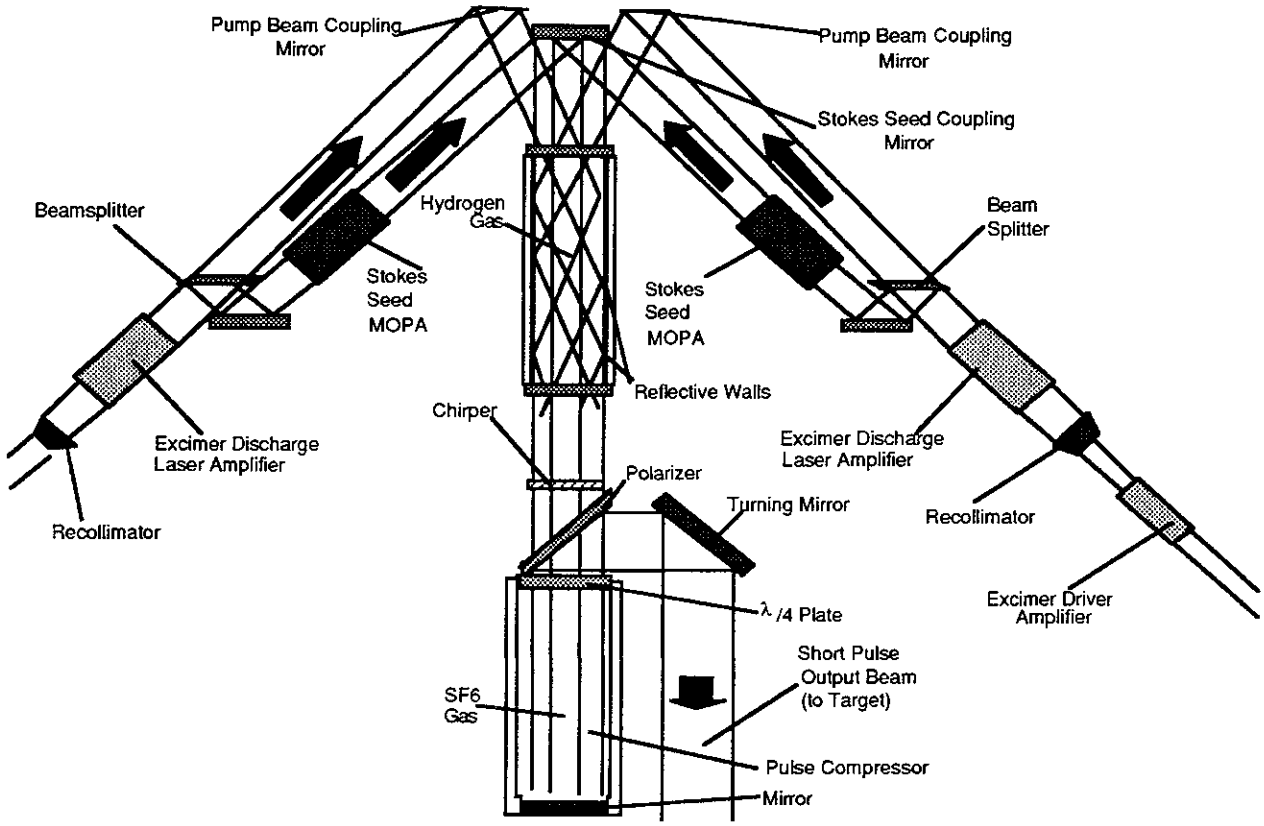

Figure 4.2.2-9 The SBS Pulse Compressor is Readily Integrated into the Reactor Driver System Following the Raman Accumulators

In order to explore the capabilities of the SBS pulse compressor for delivering a variety of output Stokes pulse shapes to meet target compression requirements, a series of calculations were carried out using a series of different temporal "chirped" SBS seed pulse shapes. Examples of the input Stokes pulse shapes used in these simulations are shown in Figure 4.2.2-10.

In Figure 4.2.2-10, the ratios indicated are the final powers in the SBS Stokes Seeds to the initial powers. Thus, a ratio of 10^4:1 indicates that the power of the Stokes seed increases by a factor of 10,000 during the course of the nominal 10 ns Stokes seed pulse duration. The variation of spontaneous SBS linewidth with SF_6 density is important to calculate.

Using experimental data[18] substituted into Eq. 4.2.2-7, the spontaneous SBS linewidth, Γ_B, is calculated as a function of the SF_6 density with the results plotted in Figure 4.2.2-11.

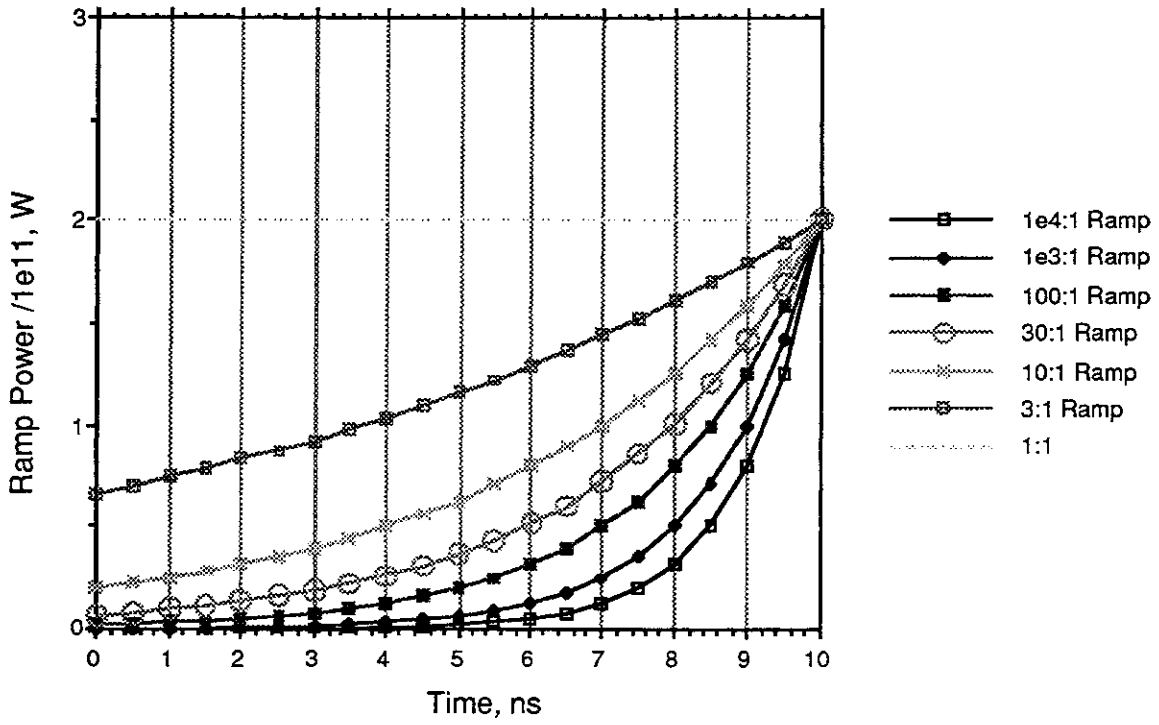

Figure 4.2.2-10 By Selecting Various Temporal Ramp Pulse Shapes for "Chirped" SBS Stokes Seeds a Variety of Compressed Pulse Shapes Can Be Generated

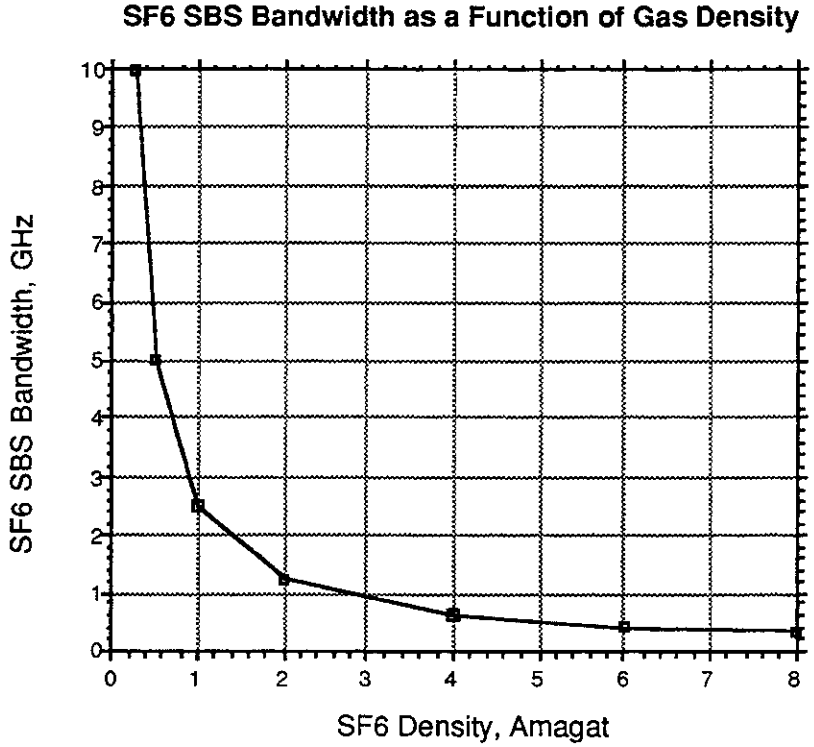

Figure 4.2.2-11 The Dependence of Spontaneous SBS Linewidth with SF_6 Density Defines Limitations on the Compressed Pulse Bandwidth

Our design point is taken near ρ = 1 amagat for SF_6 in order to trade off sufficient Brillouin gain together with adequate bandwidth (assuming an excimer/Raman pump beam bandwidth of approximately 10 GHz). From Eq. 4.2.2-7, it is evident that higher densities of SF_6 lead to increased SBS gain but over a narrower bandwidth.

Simulations of the SBS pulse compression process were carried out using the assumptions summarized in Table 4.2.2-1:

Table 4.2.2-1
Parameters Appropriate for SBS Pulse Compressor Calculations

Parameter	
Pulse Duration of Long Excimer Laser Pulse:	τ_{laser} =250 ns
Energy in Long Raman Accumulator Pulse:	E = 120 kJ
Type of SBS Gain Medium:	SF_6
Pressure of SBS Gain Medium:	2 amagat
Bandwidth of Excimer Laser Pulse:	5 GHz
SBS Stokes Seed Frequency Shift:	98 GHz
Quantum Efficiency:	99.9%
Length of SBS Cell = $c\tau_{laser}/2$	38 m
Pulse Length of Compressed Pulse:	see below
Conversion Efficiency:	see below

The effective pulse lengths and conversion efficiencies of the simulated output pulses from the SBS cell depended upon the shape of the Stokes seed used. Results of these calculations illustrating examples of the different output pulse shapes generated by the example SBS pulse compressor cell are shown in Figure 4.2.2-12.

The efficiencies of the pulse compressors as functions of ramp ratios are illustrated in Figure 4.2.2-13 for 1 amagat SF_6 and 1 meter aperture SBS cells.

Additional increases in conversion efficiency can be achieved by optimization of gas density, cell aperture, and SBS medium used. Since the calculated SBS pulse compression efficiencies depend upon the shape of the output Stokes pulse, it is necessary to specify the temporal shape of the output Stokes pulse in order to define a specific SBS conversion efficiency. Examples of ouptut Stokes pulse shapes are triangular, rectangular, etc. Use of a "picket fence" series of short output pulses synthesizing the main compression pulse can permit a significant increase in the SBS conversion efficiency up to the limit of the quantum efficiency of >99%. Without a more precise definition of the required pulse shape, the design point selection must remain imprecisely defined.

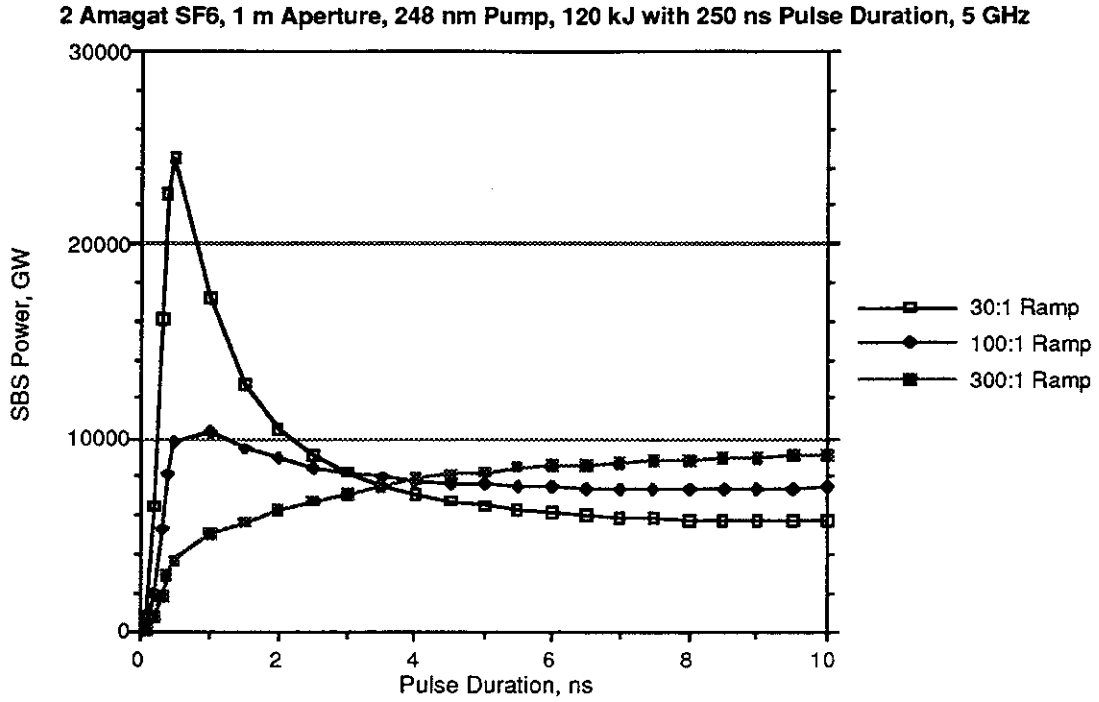

Figure 4.2.2-12 A Variety of Output SBS Pulse Shapes in SF_6 as Functions of SBS Stokes Seed Ramp Ratios is Available for D/T Target Compression

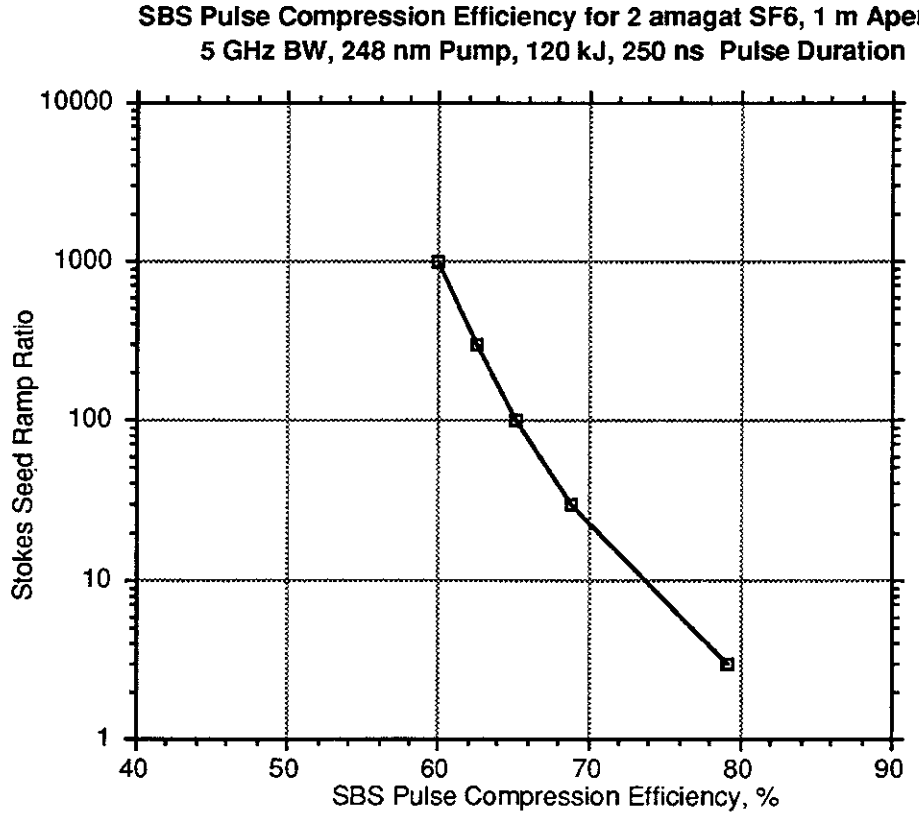

Figure 4.2.2-13 The SBS Conversion Efficiency Depends on SBS Seed Ramp Ratios

4.2.2.4 Summary of Laser Beam Conditioning Strategies - The approach for designing the KrF laser driver for a circa 2030 inertial fusion energy (IFE) power plant was to optimize the performance, efficiency, reliability, safety, and cost effectiveness of the excimer laser amplifiers independently of the DT target pellet irradiation requirements. Since optimized excimer lasers (OELs) are likely to produce ultraviolet laser pulses that are too low in energy (E ~ 3-5 kJ) to meet the IFE pellet requirement of E_{pulse} ~ 5 MJ, and with pulses that are much too long (λ_{laser} ~ 250 ns) for estimated ideal target compression scenarios using 6 ns pulses, a fundamental aspect of our design strategy is to design coherent laser beam accumulators to collect a sufficient number (~2000) of OEL beams in order to achieve the requisite 5 MJ energy level while using integated pulse compressors to generate the needed 6 ns pulse durations. Although there are conventional techniques for incoherent beam combination and angular multiplexing for pulse compression, two non-linear optical techniques for achieving coherent beam combination and pulse compression were selected because of their inherent simplicity, flexibility, and outstanding performance capability.

The non-linear optical architectures selected for achieving coherent beam combination and pulse compression are the forward rotational stimulated Raman scattering in hydrogen (for beam combination)[10,15] and the backward-seeded stimulated Brillouin scattering[17] in SF_6 (for pulse compression). Computer simulations were used to estimate the performance of each of these systems. The forward Raman conversion should have an efficiency of 90% and the SBS pulse compression from 70% to 95%, depending upon whether the main laser pulse format is a single 6 ns pulse or a 6 ns pulse synthesized from a series of "picket fence" composed of shorter pulses. Longer, flat-topped monolithic SBS Stokes output pulses are achieved in this design at the expense of conversion efficiency. Higher order Stokes conversion in the Raman accumulators is controlled by limiting both the H_2 path length in the cells and minimizing the angle, θ, between the pump and Stokes beams to control ASE seeding higher order Stokes beams.

By selecting both H_2 and SF_6 pressures near 1 atmosphere, no dangers associated with high pressure optical cells occur. The electric discharge excimer lasers are operated at relatively low voltages producing minimal x-ray hazards. The Raman accumulators are pumped with atmospheric pressure electric discharge excimer lasers producing only a few kilojoules each and the failure modes of the electric discharge excimer lasers are non-catastrophic. This architecture also permits further development of potentially efficient ArF (λ_{laser} = 193 nm) excimer laser amplifier modules. Use of vibrational H_2 or D_2 transitions in the Raman accumulators could be used to shift the wavelength out to λ = 210 nm. This laser driver architecture emphasizes safety, reliabilty, and efficient operation in wavelengths that couple well with the targets.

References for 4.2

1. "Inertial Confinement Fusion Reactor Design Studies Recommended Guidelines," prepared for the Department of Energy Office of Fusion Energy, Dr. Ronald C. Davidson (Chairman), Massachusetts Institute of Technology, Cambridge, MA, September 1990.

2. "Electron-Beam Sources for Pumping Large Aperture KrF Lasers," Louis A. Rosocha and Kenneth B. Riepe, Fusion Technology 11, pp. 576-611 (1987).

3. "Performance of the Aurora KrF ICF Laser System," J. E. Jones, et al., Proceedings of the International Conference on Lasers '89, pp. 88-95, 3-8 December 1989.

4. "Aurora Multi-kilojoule KrF Laser System Prototype for Inertial Confinement Fusion," Louis A. Rosocha, *et al.*, Fusion Technology 11, pp. 497-531 (1987).

5. "KrF for Fusion: An Overview of Laser Issues," Reed Jensen, Fusion Technology 11, pp. 497-531 (1987).

6. "Design of a 100 kJ KrF Power Amplifier Module," J. Allan Sullivan, Fusion Technology 11, pp. 684-704 (1987).

7. "The Aurora Laser Optical System," John A. Hanlon and John McLeod, Fusion Technology 11, pp. 636-653 (1987).

8. "Aurora Multi-kJ KrF Laser System Prototype for Inertial Confinement Fusion," Louis A. Rosocha, et al., Fusion Technology 11, pp. 497-531 (1987).

9. "Future Developments and Applications of KrF Laser-Fusion Systems", David B. Harris, et al., Fusion Technology 11, pp. 705-731 (1987).

10. "New Techniques for KrF Laser Fusion Systems," M. J. Kushner, J. J. Ewing, J. M. Egglestron, D. B. Lowenthal, R. G. Berger, Interim Report for the Los Alamos National Laboratory, Spectra Technololgy, Inc., Seattle, WA (1985).

11. "Raman Pulse Compression of Excimer Lasers for Application to Laser Fusion, " J. R. Murray, et al., IEEE J. Quant. Elect., QE-15, pp342-368 (1979).

12. "Optical Pulse Compressor Systems for Laser Fusion, " J. J. Ewing, et al., IEEE J. Quant. Elect., QE-15, pp368-379, (1979).

13. "Beam Combination through stimulated Brillouin scattering,", Richard H. Moyer, et al., JOSA, 5 pp. 2473--2489 (1988).

14. "Raman Beam Combining Program," Final Report for Contract #F29601-85-C-0053, prepared for the Air Force Weapons Laboratory, Kirtland Air Force Base, New Mexico, Shirley J. Pfeifer, K. Allardyce, R. Johnson, G. Linford, H. Injeyan, and J. Betts, TRW Applied Technology Division, Redondo Beach, CA, and H. Komine, G. Lombardi, W. Long, and E. Stappaerts, Northrop Research & Technology Center, Palos Verdes Peninsula, CA, September 1986.

15. "Raman Oscillator Studies," Final Report for Contract F29601-84-C-0051, prepared for AFCMD, Kirtland Air Force Base, New Mexico, Jerry Oldenettel and Michael Terpka, Western Research Corporation, San Diego, CA, March 1987.

16. Laser Handbook, edited by F. T. Arecchi, North-Holland Book Co., W. Kaiser, M. Maier, "Stimulated Rayleigh, Brillouin, and Raman Spectroscopy," pp. 1116-1120.

17. "Optical Methods for Laser Beam Control," Arthur A. Mak and Leonid N. Soms, Proceedings of SPIE, Vol. 1415, Modeling and Simulation of Laser Systems II, pp. 110-119, (1991).

18. "Direct Measurement of the Acoustic Decay Times of Hypersonic Waves Generated by SBS," M. J. Damzen, M. Hutchinson, & W. Schroeder, IEEE J. of Quant. Electronics QE-23, pp. 328-334 (1987).

4.3 Rationale for Heavy Ion Driver Options

The configuration of the Prometheus-H Heavy Ion Driver was significantly influenced by the projected cost of electricity of the plant. Two key design choices for the simplification of the driver were the substitution of a single beam LINAC plus storage rings for the multiple beam LINAC and the channel transport of the entire beam through a single small aperture in the first wall/blanket rather than through many large apertures.

4.3.1 Single Beam LINAC Plus Storage Rings Vs. Multiple Beam LINAC - The total energy requirements for the target are such that many beamlets must be accelerated and combined. The major cost drivers in the accelerator are the quadrupole focusing magnets that contain the beamlets, the induction cores that maintain the acceleration gradient for the duration of the pulse, and the pulsed power systems that provide the total energy gain for all of the beamlets.

In the case of a multiple beam LINAC, there are N beamlets per reactor shot to be accelerated in parallel. The cross-sectional area is proportional to N, as in Figure 4.3.1-1.

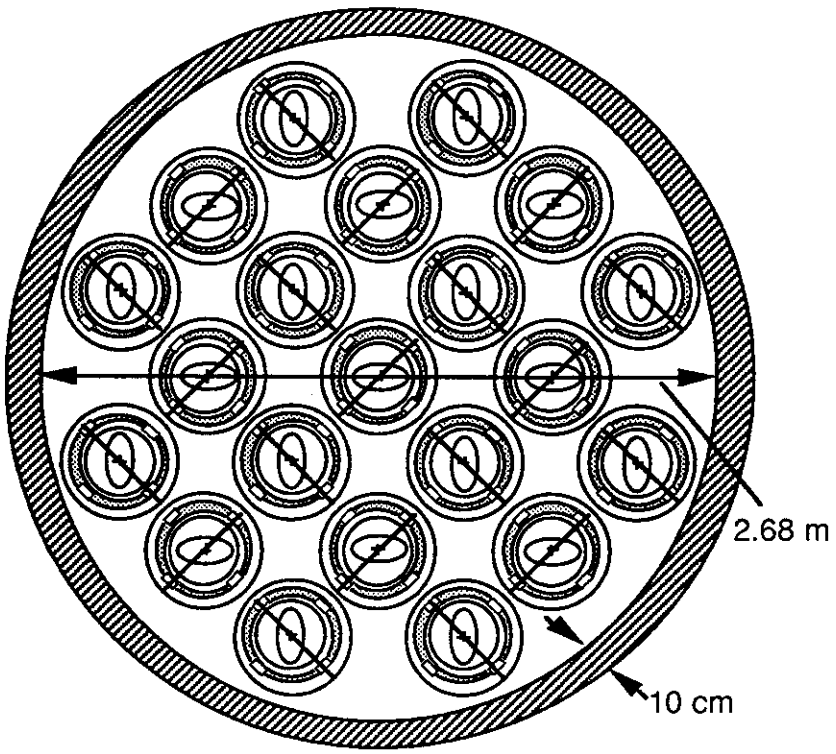

Figure 4.3.1-1 Multiple Beam LINAC Cross-Section

In the multiple beam LINAC, there are N magnets per unit length in order to confine each beamlet. The induction core that surrounds the magnets has a thickness, t, to provide the required volt-seconds (voltage/meter x pulse length = ΔB x area/meter = t), so the volume of the core is $2 \pi N^{1/2}$ t. The total energy supplied by the pulsed power is the beam energy plus the losses in the cores (which are proportional to the core volume) times a factor to account for the efficiency of the pulsed power. Since beam energy is fixed by the target requirement, the variables are the core losses and the pulsed power efficiency.

In the case of a single beam LINAC, the same N beamlets per reactor shot can be accelerated serially. The cross-section for this configuration appears in Figure 4.3.1-2.

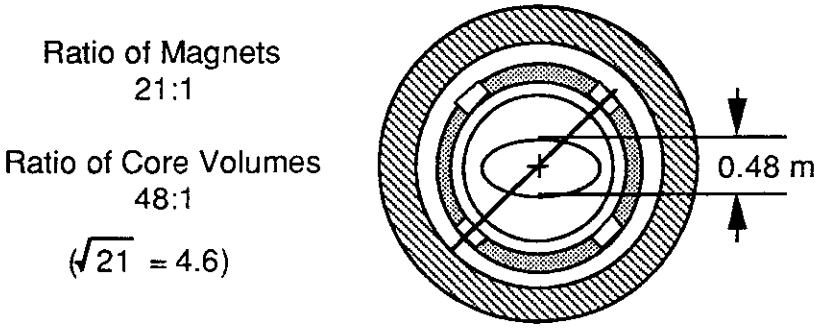

Figure 4.3.1-2 Single Beam LINAC Cross-Section

There is only one magnet per unit length, a factor of N improvement. Although the core has the same thickness, t, to provide the same number of volt-seconds, the inner radius and the core volume are reduced a factor of $N^{1/2}$. Although the core volume is reduced, the core is fired N times rather than once, leading to a net increase in the core losses per reactor shot. Total beam power is the same; therefore, there is no intrinsic reason why the efficiency of the pulsed power should change. However, the cost per joule of the pulsed power will go up due to the high repetition rate capability.

Based on the cost model, this single beam LINAC is the more cost-effective system. The technology of the single beam LINAC is more developed. The complication is that there is a time delay of the order of milliseconds between the first and last of the serially-generated beamlets. A number, N, of separate storage rings must be used to function as delay lines for the beamlets so they may arrive at the target simultaneously. The technical feasibility of storing high current ion beams for millisecond time scales must be demonstrated, since there is a possibility of instabilities. This is identified as a Critical Issue for the Heavy Ion Driver. Given that storage is feasible, the cost impact of the rings is relatively minor. Since there are no acceleration modules in the storage rings, the only cost driver is the superconducting magnets, which now include dipole bending magnets as well as quadrupole focusing magnets. Thus, the total number of magnets in all of the storage rings is roughly equal to the number in the final 10% of

the multiple beam LINAC. Even with the storage rings added to the LINAC, the much lower cost associated with the single beam system yields a more attractive driver for the 1000-MWe power reactor.

4.3.2 Pinched Channel Transport Vs. Ballistic Focusing - The indirect drive target is illuminated from two sides with proper access for the beams through the shielding, blanket, and first wall elements. Following the target implosion, neutrons and gas flow out of the access ports, back toward the final focus magnetic optics and the rest of the linear accelerator with concomitant damage and contamination of those elements.

The superconducting final focus magnets are susceptible to damage from the neutrons with little room for shielding. More robust, iron-dominated, room temperature quadrupoles are available; however, they are large, inefficient, and expensive. At 2 MW electrical per normal conducting quadrupole lens (the value used for HIBALL-II[1]) the reactor power balance is skewed since this is roughly the time-averaged kinetic power per beamlet in Prometheus-H.

The gas load is also a problem since, within the reactor chamber, the partial pressure of the noncondensibles (primarily hydrogen) is about 100 mtorr just before a shot, and it peaks at hundreds of torr soon after. This gas leaves the chamber primarily through pumps but also through the target chamber apertures, where it heads back toward the accelerator. The accelerator must be kept in the 10^{-7} to 10^{-10} torr regime for beam propagation. There is strong motivation to keep the number and size of apertures small. There are two scenarios possible in the relatively low energy ($E < 10$ GeV) and high charge ($Q > 1$) regime.

The first case, ballistic focusing, is illustrated in Figure 4.3.2-1. Each of N beamlets can come through a 20 to 40 cm diameter hole in the reactor wall, individually focussed on the target by its final focus magnets. The beams propagate approximately 5 m through whatever gas is within the target chamber, which includes both burn products and additives. The beamlet must be at least partially neutralized to overcome space charge repulsion, and although there is presumably plenty of plasma within the beam duct to provide electrons, this plasma will also collisionally strip the beam ions to higher charge states. The beam is entirely within the target chamber before the first ion strikes the target. The precursor beamlets (containing one-fourth to one-third of the beam power) continue to strike the target for 30 to 40 ns before the rest of the beamlets arrive, generating x-rays that photo-ionize the beam, further increasing the beam charge state and interfering with the space-charge neutralization process that permits focusing to small spot sizes. After ignition, the neutrons and gas head back up the ducts to the magnets and the rest of the accelerator.

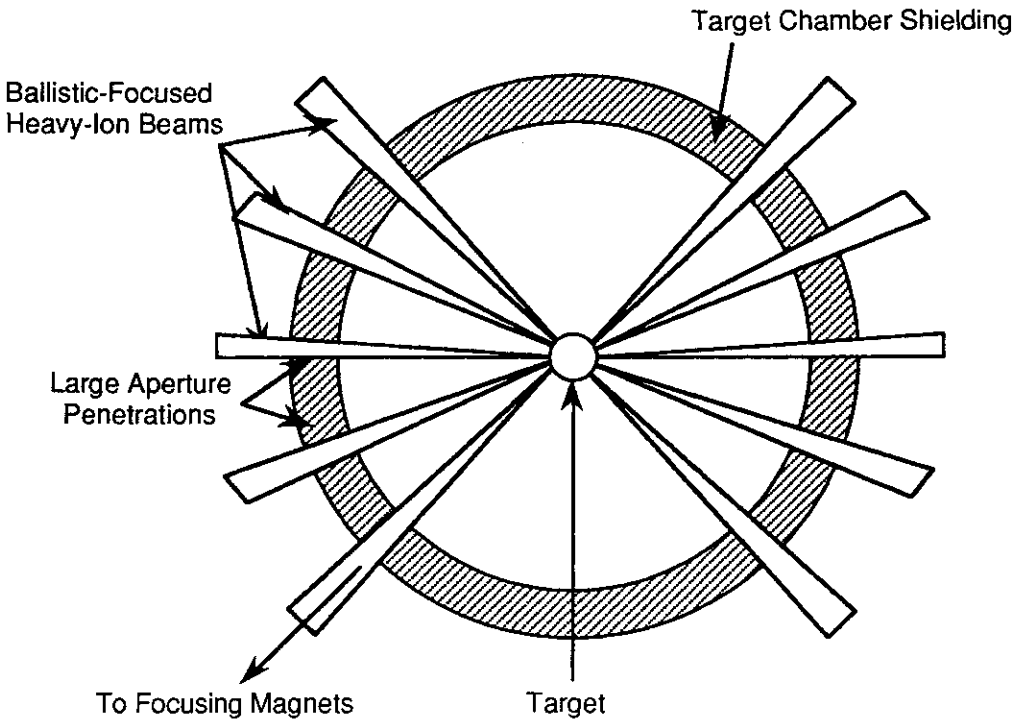

Figure 4.3.2-1 Ballistic Focusing of HI beams

The second case, pinched channel transport, is illustrated in Figure 4.3.2-2. The beamlets again focus down from 20 to 40-cm diameters, but are now directed to a common spot outside the blanket rather than the target pellet. The region they traverse has a controlled amount of gas or plasma, permitting fine tuning to control the degree of neutralization and collisional stripping. The beam ions converge on a thin layer of gas at the outside of the blanket, completely stripping ($Q > 50+$ within a few millimeters) and increasing the beam electrical current by a very large factor. The envelope begins to collapse under the influence of the pinch current, overcoming the tendency of the outer beamlets to separate. The coalesced beam propagates to the target through a 2-cm diameter hole in the blanket. Because the ions are already completely stripped, the x-rays caused by the precursor have no effect. After ignition, the small flow of backstreaming gas through the 2-cm aperture is blocked by the same gas layer that stripped the beam ions. There is room to add additional shielding for the magnets to protect them from neutrons that pass through the ducts in the main shielding.

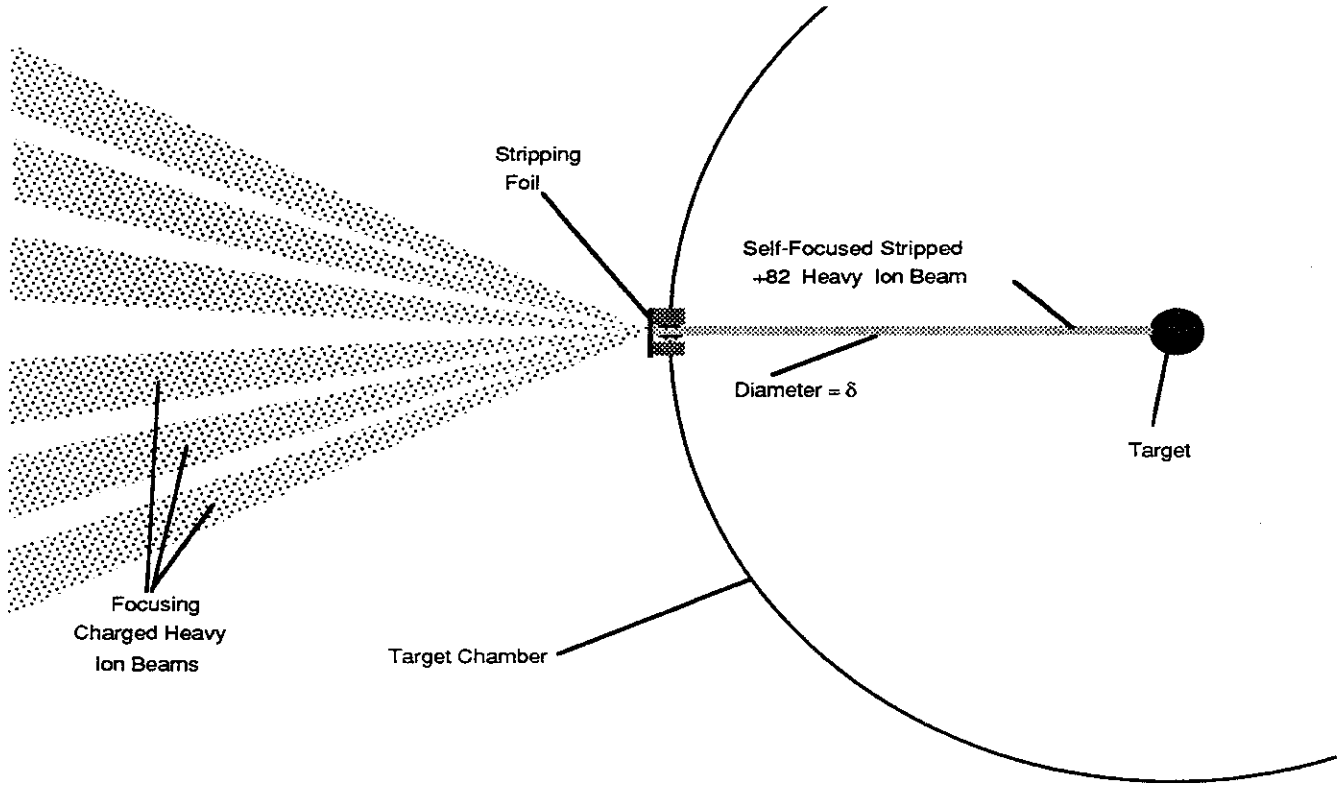

Figure 4.3.2-2. Pinched Channel Transport in Target Chamber

Both methods rely on the detailed response of the plasma and are, therefore, speculative. Neither has been demonstrated with anything approaching a relevant heavy ion beam. Some computer simulations have indicated the beam pinch will not form, but contrary results are obtained when different input conditions are assumed. Although the pinched channel transport is probably riskier, the engineering advantages it affords make it worthwhile to carry along as a baseline until a relevant experiment can be performed.

References for 4.3

1. B. Badger, et al., "HIBALL II - An Improved Conceptual Heavy Ion Beam Driven Fusion Reactor Study," UWFDM-450/KfK 3840 , Fusion Engineering Program, University of Wisconsin (July 1985).